Desalination 308 (2013) 56–62

Contents lists available at ScienceDirect

Desalination

journal homepage: www.elsevier.com/locate/desal

Falling film evaporation with polymeric heat transfer surfaces

Jochen B.P. Christmann [1], Lorenz J. Krätz, Hans-Jörg Bart *

Chair of Separation Science and Technology, TU Kaiserslautern, P.O. Box 3049, 67653 Kaiserslautern, Germany

ARTICLE INFO

Article history:
Received 8 March 2011
Received in revised form 9 May 2011
Accepted 10 May 2011
Available online 12 June 2011

Keywords:
Falling film
Evaporation
Heat transfer
Polymer
Polyetheretherketone

ABSTRACT

The corrosive process conditions in common multi-effect distillation (MED) plants require heat transfer surfaces consisting of high-grade metal alloys. However, corrosion resistant polymers can be a reasonable alternative to expensive metals. But it is necessary to use thin polymer films, which must be mechanically stabilized by a spacer grid, to compensate the low thermal conductivity of polymers. A falling film plate evaporator with heat transfer surfaces made out of the high performance polymer polyetheretherketone (PEEK) was already developed based on those considerations. Experimentally measured overall heat transfer coefficients with the prototype heat exchanger at MED process conditions are presented in this publication. They are comparable to typical values of metallic falling film heat exchangers. Furthermore, the heat transfer within the prototype heat exchanger was modeled and compared with the obtained experimental results. It will be shown that correlations valid for falling film heat transfer on a vertical wall are not applicable for a spacer stabilized polymeric heat transfer surface, but they can be used after modifications.

1. Introduction

Low temperature multi-effect distillation (MED) is an established process in seawater desalination. Maximum temperatures usually do not exceed 70 °C [1]. Additionally, MED plants with cocurrent vapor/brine flow show low pressure differences between the two sides of the heat transfer surface in each effect. Nevertheless, the high corrosivity of hot seawater demands heat transfer surfaces made of corrosion resistant and expensive metal alloys [2]. Because of the low process temperatures and pressure differences, polymeric heat transfer surfaces could be a cost effective and corrosion resistant alternative to metallic materials in the cocurrent MED process. Therefore, a prototype falling film plate heat exchanger was designed using polyetheretherketone (PEEK) as heat transfer surface material [3]. PEEK is highly resistant against hydrolysis and it offers excellent mechanical properties, also at elevated temperatures [4]. In this study falling film heating and evaporation on PEEK heat transfer surfaces at typical MED process conditions was investigated, to proof the applicability of polymeric heat transfer surfaces in MED plants. Furthermore, heat transfer within the prototype heat exchanger was modeled to provide a theoretical basis for prospective thermal design.

One drawback of polymeric heat transfer surfaces is the low thermal conductivity of polymers. The thermal conductivity of PEEK is only 0.25 W/(m K), compared to 15 W/(m K) for stainless steel and 52 W/(m K) for CuNi 90/10. But the thermal conductivity of polymer films might be increasing due to water uptake of the polymer matrix [5]. Nevertheless, it is necessary to use thin PEEK films of about 25 μm thickness to get a thermal resistance for conduction of the heat transfer surface, which is comparable to metallic materials and to avoid an increase of the required heat transfer area. An approach of using thin polymer films as heat transfer surfaces in the MED process was already described by Scheffler and Leao [6]. They have used 20–50 μm thick polyethylene and polypropylene films, which were welded and arranged in a horizontal tube like manner. Another possibility to reduce the thermal resistance of polymeric heat transfer is to increase the polymer's thermal conductivity. This could be achieved by addition of fillers to the polymer matrix [7,8].

Besides thermal conductivity and wall thickness, also the heat transfer coefficients for condensation h_{cond} and for heating h_{heat} or evaporation h_{evap} contribute to the mean overall heat transfer coefficient U and have to be taken into consideration (Eq. (1)).

$$\frac{1}{U} = \frac{1}{h_{cond}} + \frac{S}{k_{wall}} + \frac{1}{h_{heat\,/\,evap}} \tag{1}$$

The thermal resistances are reciprocal values of the terms in Eq. (1). It follows that 1/U equals the total thermal resistance (R_{tot}), $1/h$ is the thermal resistance for condensation, heating or evaporation ($R_{cond/heat/evap}$) and S/k_{wall} corresponds to the thermal resistance of conduction. (R_{cond}). It should be mentioned for the sake of completeness, that fouling is neglected and the thermal resistances mentioned in this publication are area related thermal resistances with the dimension m² K/W.

* Corresponding author. Tel.: +49 631 205 2414; fax: +49 631 205 2119.
E-mail address: bart@mv.uni-kl.de (H.-J. Bart).
[1] Present address: Julius Montz GmbH, Werner-Heisenberg-Straße 13, 76829 Landau, Germany.

0011-9164/$ – see front matter © 2011 Elsevier B.V. All rights reserved.
doi:10.1016/j.desal.2011.05.027

2. Experimental set-up

The prototype falling film plate heat exchanger with polymeric heat transfer surfaces is shown in Fig. 1. It consists of condensation and evaporation elements, which are arranged alternating and which are separated by PEEK films as heat transfer surfaces (b = 0.5, L = 1 m). Four heat transfer surfaces ($n = 4$) with a total heat transfer area of 2 m² were used. A spacer grid is placed into the evaporation elements to stabilize the PEEK film against the pressure difference between condensation and evaporation side of the heat transfer surface. The spacer consists of a spot welded square mash grid (stainless steel) with a rod diameter of 3 mm and a grid size of 30 × 30 mm. The horizontal rods are in direct contact with the PEEK film (Fig. 2). Heating steam and brine enter the heat exchanger at the top. Brine is appliqued as a falling film and flows over the spacer grid where it is heated to boiling temperature and evaporated. The falling film feed was provided beneath boiling temperature at the inlet to exclude flash evaporation effects that would disturb proper heat and mass balancing. Saturated heating steam is provided in excess to avoid condensate subcooling. Condensate, excess heating steam, brine and vapor leave the heat exchanger at the bottom. Volume flows of falling film liquid and condensate entering or leaving the heat exchanger, as well as their temperatures are measured by magneto-inductive or ultrasonic flow meters and Pt100 thermometers, respectively, for mass and energy balancing. The design of the prototype heat exchanger, spacer, pilot plant and measuring technique for estimating the overall heat transfer coefficients was already published and precisely described in [3].

PEEK films aptiv 1000 from Victrex plc. (unreinforced, semi crystalline) with a wall thickness of 25 μm are used as heat transfer surfaces. With respect to the thermal resistance this corresponds to about 1.5 mm thick stainless steel. PEEK films were purchased one-side plasma treated (falling film side) to enhance their wetting behavior with water. The heat transfer surface was checked for complete wetting with the falling film at the experimental liquid load before heat transfer experiments. Saturated steam served as heating steam. Distilled water was used as falling film liquid. To permit magneto-inductive flow metering, electrical conductivity was adjusted with NaCl to approximately 30 μS/cm. The objective of this work is the heat transfer performance and not the corrosion properties of the heat exchanger. Thus synthetic seawater was not used to avoid boiling point elevation during evaporation and to allow for proper energy balancing. Error bars and intervals represent 68% confidence intervals including statistical variation and measuring inaccuracy of the measuring devices due to error propagation.

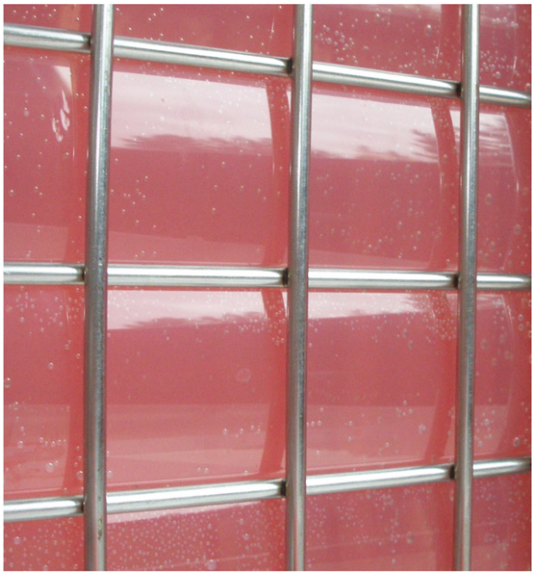

Fig. 2. PEEK film heat transfer surface and spacer grid.

3. Heat transfer analysis and modeling

The temperature dependence of the properties of water and steam was taken into account. For this purpose, the material properties were taken from appropriate literature [9–11] and approximated by polynomial functions of the 4th degree with respect to temperature.

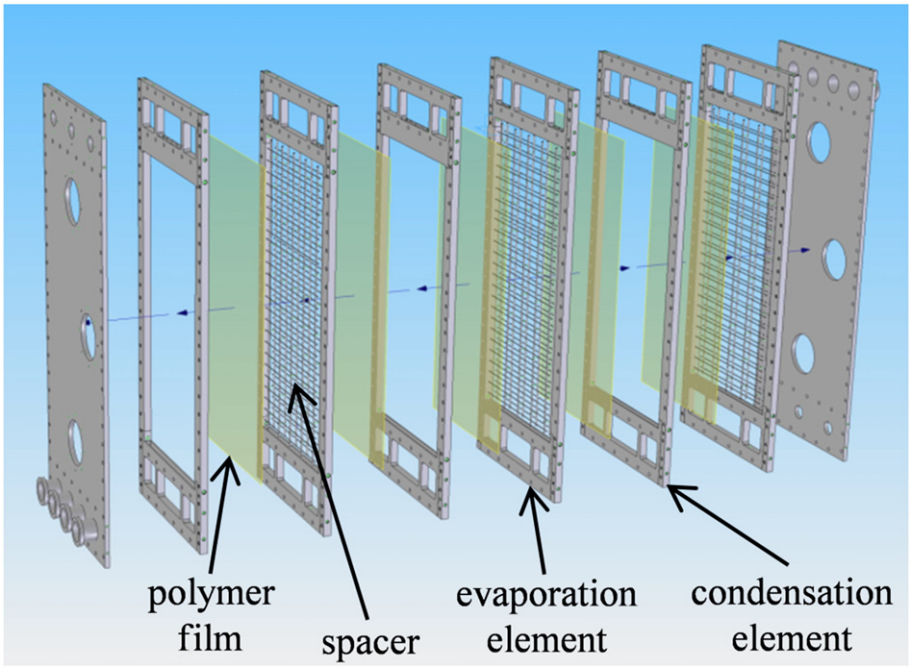

Fig. 1. Exploded assembly drawing of the falling film plate heat exchanger with PEEK film heat transfer surfaces and spacers.

3.1. Experimental heat transfer analysis

The total heat flow through the heat transfer surface is described by Eq. (2).

$$Q = U \cdot A \cdot \Delta\vartheta \tag{2}$$

The temperature difference has to be calculated with respect to the heat transfer instance on the falling film side of the heat exchanger. The logarithmic mean temperature difference for cocurrent flow is used for falling film heating (Eq. (3)), whereas a simple mean temperature difference is applied during falling film evaporation (Eq. (4)). It is assumed that no condensate subcooling and no boiling point elevation are present, which is leading to a constant condensation temperature ϑ_{cond} and a constant evaporation temperature ϑ_{evap}.

$$\Delta\vartheta = \Delta\vartheta_{log,\,mean} = \frac{\left(\vartheta_{cond} - \vartheta_{heat,\,min}\right) - \left(\vartheta_{cond} - \vartheta_{heat,\,max}\right)}{\ln\left(\frac{\left(\vartheta_{cond} - \vartheta_{heat,\,min}\right)}{\left(\vartheta_{cond} - \vartheta_{heat,\,max}\right)}\right)} \tag{3}$$

$$\Delta\vartheta = \Delta\vartheta_{mean} = \vartheta_{cond} - \vartheta_{evap} \tag{4}$$

When the falling film is preheated prior to evaporation from minimum temperature at the inlet $\vartheta_{heat,min}$ to maximum heating temperature $\vartheta_{heat,max}$, the maximum heating temperature equals the evaporation temperature ϑ_{evap}. Eqs. (5)–(7) are employed to determine the experimental mean overall heat transfer coefficient $U_{exp,mean}$, taking heating (Q_{heat}) and evaporation (Q_{evap}) of the falling film into account.

$$U_{exp,\,mean} = \frac{|Q_{heat}|}{A \cdot \Delta\vartheta_{log,\,mean}} + \frac{|Q_{evap}|}{A \cdot \Delta\vartheta_{mean}} \tag{5}$$

$$Q_{heat} = \dot{m}_{FF} \cdot c_{p,\,L} \cdot \left(\vartheta_{heat,\,max} - \vartheta_{heat,\,min}\right) \tag{6}$$

$$Q_{evap} = -\dot{m}_V \cdot \Delta h_V \tag{7}$$

3.2. Heat transfer modeling

The experimental results are used as basis for modification of established heat transfer correlations. This was done by modeling of the heat transfer and adaption of established correlations to the experimental values. Furthermore, the heat transfer modeling was done to get a deeper insight and understanding of the heat transfer within the prototype polymer film plate heat exchanger.

3.2.1. Mass and energy balances

Ordinary differential equations (ODE) are used to establish one-dimensional steady state mass and energy balances for heat transfer modeling. Axial heat conduction, pressure drop as well as kinetic and potential energies are neglected. It is assumed that gas and liquid phases are in thermal equilibrium and no temperature gradient is present within the liquid film normal to the heat transfer surface.

Steady state mass balances of the condensate film and the falling film are given in Eqs. (8) and (9), respectively. The first term represent the volume related mass flow of the liquid film along the x-coordinate. The second term describes the mass flow change due to condensation or evaporation ($\vartheta_{FF} = \vartheta_{boiling}$), respectively. An energy balance for the condensation side is dispensable, because the condensate film temperature is assumed to be constant. The energy balance for temperature calculation of the falling film is given by Eq. (10). The first term represent the falling film temperature change, whereas the second term describes the heat transfer to the falling film in the case of falling film heating ($\vartheta_{FF} < \vartheta_{boiling}$).

The equations are coupled by the heat transfer term and the temperature. Eqs. (8)–(10) reveal that no mass balance, but an energy balance is required for the heating of the falling film, because of constant mass flow and varying falling film temperature. In contrast, a mass balance but no energy balance is needed to describe an evaporation of the falling film, since the evaporation temperature is constant and the mass flow is decreasing.

$$0 = \frac{\partial(u_{CF} \cdot \varepsilon_{CF} \cdot \rho_{CF})}{\partial x} - \frac{U \cdot a_{cond} \cdot (\vartheta_{CF} - \vartheta_{FF})}{\Delta h_{V,\,cond}} \tag{8}$$

$$\begin{aligned} 0 &= \frac{\partial(u_{FF} \cdot \varepsilon_{FF} \cdot \rho_{FF})}{\partial x} && for \quad \vartheta_{FF} < \vartheta_{boiling} \\ 0 &= \frac{\partial(u_{FF} \cdot \varepsilon_{FF} \cdot \rho_{FF})}{\partial x} + \frac{U \cdot a_{evap} \cdot (\vartheta_{CF} - \vartheta_{FF})}{\Delta h_{V,\,evap}} && for \quad \vartheta_{FF} = \vartheta_{boiling} \end{aligned} \tag{9}$$

$$\begin{aligned} 0 &= -\left(u_{FF} \cdot \varepsilon_{FF} \cdot \rho_{FF} \cdot c_{p,\,FF}\right) \cdot \frac{\partial \vartheta_{FF}}{\partial x} \\ &\quad + U \cdot a_{evap} \cdot (\vartheta_{CF} - \vartheta_{FF}) && for \quad \vartheta_{FF} < \vartheta_{boiling} \\ 0 &= -\left(u_{FF} \cdot \varepsilon_{FF} \cdot \rho_{FF} \cdot c_{p,\,FF}\right) \cdot \frac{\partial \vartheta_{FF}}{\partial x} && for \quad \vartheta_{FF} = \vartheta_{boiling} \end{aligned} \tag{10}$$

Eqs. (11)–(13) depict the boundary conditions of the ODE system for condensate and falling film mass flows and falling film temperature.

$$(u_{CF} \cdot \varepsilon_{CF} \cdot \rho_{CF})\,|_{x=0} = \frac{\dot{m}_{CF,\,in}}{n \cdot b \cdot \frac{c_{cond}}{2}} = 0 \tag{11}$$

$$(u_{FF} \cdot \varepsilon_{FF} \cdot \rho_{FF})\,|_{x=0} = \frac{\dot{m}_{FF,\,in}}{n \cdot b \cdot \frac{c_{evap}}{2}} \tag{12}$$

$$\vartheta_{FF}\,|_{x=0} = \vartheta_{FF,\,in} \tag{13}$$

Mass flows of the liquid films result from Eqs. (14) and (15). Assuming no condensate or vapor flow at the inlet, the absolute mass flows of the gas phase (vapor) can be calculated according to Eqs. (16) to (17).

$$\dot{m}_{CF} = \frac{c_{cond}}{2} \cdot b \cdot n \cdot (u_{CF} \cdot \varepsilon_{CF} \cdot \rho_{CF}) \tag{14}$$

$$\dot{m}_{FF} = \frac{c_{evap}}{2} \cdot b \cdot n \cdot (u_{FF} \cdot \varepsilon_{FF} \cdot \rho_{FF}) \tag{15}$$

$$\dot{m}_S = \dot{m}_{S,\,in} - \dot{m}_{CF} \tag{16}$$

$$\dot{m}_V = \dot{m}_{FF,\,in} - \dot{m}_{FF} \tag{17}$$

The hold-up ε can be determined with the liquid film thickness by applying Nusselt's water skin theory [12,13]. The volume related heat transfer surface, as well as overall heat transfer coefficients are calculated according to Eqs. (18) to (19) and (1), respectively.

$$a_{cond} = \left(\frac{c_{cond}}{2}\right)^{-1} \tag{18}$$

$$a_{evap} = \left(\frac{c_{evap}}{2}\right)^{-1} \tag{19}$$

3.3.2. Heat transfer coefficients

Liquid load (Eq. (20)), Reynolds number of the liquid film (Eq. (21)), Prandtl number (Eq. (22)) and Nusselt number (Eq. (23)) are needed for determination of empirical heat transfer coefficients [10].

$$\Gamma = \frac{\dot{m}_L}{n \cdot b} \tag{20}$$

$$Re_F = \frac{\Gamma}{\eta_L} \tag{21}$$

$$Pr = \frac{\eta_L \cdot c_{p,\,L}}{k_L} \tag{22}$$

$$Nu = \frac{h}{k_L} \cdot \left(\frac{\nu_L^2}{g}\right)^{\frac{1}{3}} \tag{23}$$

The following correlations refer to heat transfer on a vertical plane wall without taking shear forces between gas and liquid phase into account. Film condensation is assumed and therefore the local Nusselt number for condensation is estimated based on a laminar condensate film according to Nusselt's water skin approach (Eq. (24)) [12,13].

$$Nu_{cond} = 0.693 \cdot \left(\frac{1-\frac{\rho_G}{\rho_L}}{Re_{F,\,CF}}\right) \tag{24}$$

Eqs. (25)–(28) describe the Nusselt number for of falling film heating or cooling at different flow regimes, if a constant wall temperature is assumed. The maximum value derived by Eqs. (25)–(28) yields the heat transfer coefficient that should be applied (Eq. (29)) [10,14].

Thermally developing flow:

$$Nu_{heat,\,1} = 0.912 \cdot \left(\frac{Re_{F,FF}^{\frac{1}{3}} \cdot Pr \cdot \left(\frac{\nu_L^2}{g}\right)^{\frac{1}{3}}}{L}\right)^{\frac{1}{3}} \tag{25}$$

Laminar, hydrodynamically and thermally developed flow:

$$Nu_{heat,\,2} = 1.3 \cdot Re_{F,FF}^{-\frac{1}{3}} \tag{26}$$

Zone of transition to turbulent flow:

$$Nu_{heat,3} = 0.0425 \cdot Re_{F,FF}^{\frac{1}{5}} \cdot Pr^{0.344} \tag{27}$$

Turbulent flow:

$$Nu_{heat,4} = 0.0136 \cdot Re_{F,FF}^{\frac{2}{5}} \cdot Pr^{0.344} \tag{28}$$

Nusselt number to be chosen for estimation of the heat transfer coefficient for falling film heating:

$$Nu_{heat} = max\left(Nu_{heat,1},\ Nu_{heat,2},\ Nu_{heat,3},\ Nu_{heat,4}\right) \tag{29}$$

In the case of falling film evaporation Nusselt number is calculated according to Eqs. (30)–(32)[10,14].

Laminar flow:

$$Nu_{evap,lam} = 0.9 \cdot Re_{F,FF}^{-\frac{1}{3}} \tag{30}$$

Turbulent flow:

$$Nu_{evap,turb} = 0.00622 \cdot Re_{F,FF}^{0.4} \cdot Pr^{0.65} \tag{31}$$

Nusselt number for falling film evaporation:

$$Nu_{evap} = \sqrt{Nu_{evap,lam}^{\ 2} + Nu_{evap,turb}^{\ 2}} \tag{32}$$

The software Mathcad 2000 is used for simultaneous numerical solution of the resulting system of coupled algebraic and differential equations consisting of Eqs. (1) and (8) to (32). Discretization is done with respect to the length of the heat transfer surface (inlet: $x=0$, outlet: $x=L$) and 1000 discretization steps are used.

4. Results and discussion

4.1. Experimental heat transfer

The experimental mean overall heat transfer coefficient $U_{exp,mean}$ of the prototype heat exchanger was estimated according to Sections 2 and 3.1 in order to demonstrate the applicability of polymer film heat transfer surfaces at MED process conditions. Experimental results and corresponding process conditions are presented in Tables 1 and 2.

It can be observed that the experimental mean overall heat transfer coefficient $U_{exp,mean}$ is decreasing with increasing Reynolds number in the case of falling film heating. In contrast $U_{exp,mean}$ is increasing together with the Reynolds number when the falling film is evaporating. The comparison of $U_{exp,mean}$ at heating and evaporation reveals that evaporation leads to much higher values for $U_{exp,mean}$ than falling film heating. Since the thermal resistance of conduction R_{wall} is constant and the thermal resistance of condensation R_{cond} is assumed to be approximately the same for heating and evaporation, the change of $U_{exp,mean}$ must be caused mainly by the thermal resistance of heating R_{heat} or evaporation R_{evap}, respectively. The obtained results differ from data or correlations based on a plane wall geometry [14]. This deviation is caused by the spacer grid, which is affecting falling film hydrodynamics as well as heat transfer. Hence, it is necessary to consider the effect of the spacer grid when characterizing the heat transfer.

Achieved experimental mean overall heat transfer coefficients U_{exp} for evaporation range from 3182 to 3765 W/(m²K) in this study (Table 2). They are comparable to the values published by Kafi et al. [15], who used a related falling film plate evaporator with a metallic heat transfer surface and a spacer grid [15,16]. Kafi et al. observed values for $U_{exp,mean}$ between 2500 W/(m²K) and 3700 W/(m²K) in the second stage of their MED pilot plant [15]. Moreover, values of U for conventional metallic horizontal tube MED evaporators are in the same order of magnitude [17–19]. Comparable results for the overall heat transfer coefficient were presented by Christmann et al. with the same heat exchanger prototype, but with different polymer films [3]. Those results were achieved with polymer films, which were not wetted completely at experimental conditions. Therefore, heat transfer coefficients were theoretically extrapolated to complete wetting of the heat transfer surface. Nevertheless, the results are in good agreement with the data in the present publication, which are obtained with completely wetted plasma treated polymer films. This is indicating that the extrapolating approach used before in [3] delivered a good estimation of the overall heat transfer coefficient for complete wetting of the heat transfer surface.

The presented results demonstrate that mean overall heat transfer coefficients comparable to metallic heat exchangers can achieved not only theoretically but also practically with polymer film falling film evaporators at MED process conditions.

Table 1
Experimental mean overall heat transfer coefficients for falling film heating at atmospheric pressure.

Operating point:	Heating 1	Heating 2
Liquid load inlet Γ_{in} [kg/(m s)]	0.254 ± 0.001	0.384 ± 0.001
Reynolds number inlet $Re_{F,\,FF,\,in}$ [−]	683 ± 6	1063 ± 9
Temperature falling film inlet $\vartheta_{FF,\,in}$ [°C]	76.4 ± 0.2	79.2 ± 0.2
Temperature heating steam ϑ_S [°C]	100.6 ± 0.2	100.5 ± 0.2
Pressure difference Δp [Pa]	5059 ± 37.3	4705 ± 58.7
Exp. mean overall heat transfer coefficient $U_{exp,mean}$ [W/(m²K)]	1810 ± 47.4	1558 ± 39.5

Table 2
Experimental mean overall heat transfer coefficients for falling film evaporation at MED process conditions.

Operating point:	Evaporation 1	Evaporation 2	Evaporation 3
Liquid load inlet Γ_{in} [kg/(m s)]	0.311 ± 0.001	0.399 ± 0.001	0.506 ± 0.001
Reynolds number inlet $Re_{F,\,FF,\,in}$ [−]	608 ± 5	786 ± 7	1037 ± 9
Temperature falling film inlet $\vartheta_{FF,\,in}$ [°C]	54.1 ± 0.2	54.6 ± 0.2	57.0 ± 0.2
Temperature heating steam ϑ_S [°C]	59.0 ± 0.2	59.1 ± 0.2	60.9 ± 0.2
Pressure difference Δp [Pa]	3936 ± 26	3908 ± 26	3763 ± 26
Exp. overall heat transfer coefficient $U_{exp,mean}$ [W/(m²K)]	3182 ± 402	3285 ± 425	3765 ± 512

4.2. Heat transfer modeling

Heat transfer within the prototype heat exchanger was modeled for a better understanding of the appearing phenomena. A comparison of experimental and calculated results is shown in Table 3. The correlations for falling film heating on a plane wall (Eqs. (25)–(29)) predict the heat transfer coefficient $h_{heat,mean}$ and therefore the mean overall heat transfer coefficient U_{mean} much too high. Furthermore, the calculated heat transfer coefficient for heating is increasing with the Reynolds number when applying Eqs. (25)–(29) to the experimental conditions. This was not observed in our experiments, because the spacer grid is affecting the falling film hydrodynamics and heat transfer significantly. Raach and Mitrovic [20] as well as Salvagnini and Taqueda [21] have shown, that turbulence wires (similar to the spacers used in this publication) have a significant influence on the heat transfer coefficient in the case of falling film evaporation. Consequently, the falling film hydrodynamics and the heat transfer on the spacer stabilized polymer film are not directly comparable to a plane wall geometry. Nevertheless, Eq. (26) for laminar heating is reflecting the observed decrease of $U_{exp,mean}$ at increasing Reynolds number, which leads to the conclusion that the spacer might cause a pseudo laminar falling film flow in the case of falling film heating. In contrast to this, Eqs. (30)–(32) describe the observed relation between U and Re_F for falling film evaporation correct, but calculated values for a plane wall are too low compared to our experiments. This is also most likely based on the alternation of falling film hydrodynamics and heat transfer due to the spacer grid.

Hence, the experimental results (Tables 1 and 2) are used as basis for modification of established heat transfer correlations. A good agreement of calculated and experimental results for the mean overall heat transfer coefficient U can achieved, when Eq. (26) and Eqs. (30)–(32) for the heat transfer coefficient of the falling film are modified by adjusting the exponent of the Reynolds number. Eqs. (33) and (34) represent the modified correlations used for further calculations. Hence, Eq. (33) is replacing Eqs. (25)–(29) and Eqs. (30)–(32) are substituted by Eq. (34). The hereby obtained results are shown in Table 3. But the modified equations can only be applied to the spacer and surface geometry used in this study.

$$Nu'_{heat} = 1.3 \cdot {Re_{F,FF}}^{-0.39} \tag{33}$$

$$Nu'_{evap} = \sqrt{\left(0.9 \cdot {Re_{F,FF}}^{-0.38}\right)^2 + \left(0.00622 \cdot {Re_{F,FF}}^{0.6} \cdot Pr^{0.65}\right)^2} \tag{34}$$

Calculated mean values of the heat transfer coefficients h_{mean} based on the modified equations are displayed in Table 4 for different experimental operating points. The heat transfer coefficient for condensation h_{cond} cannot be determined exactly, because it is not clear which condensation regime is present on the polymeric heat transfer surface. Two special condensation regimes are distinguished: a) Film condensation according to Nusselt's water skin theory (Eq. (24)) [12,13]. It leads to low heat transfer coefficients (high thermal resistance) of the condensate film and it represents the worst case with respect to the thermal resistance on the condensation side. b) Droplet condensation which results in a very high heat transfer coefficient (low thermal resistance) [22,23]. In this case the thermal resistance can approximately be neglected ($h \to \infty$) at experimental conditions. The condensation phenomena depend on heat transfer surface properties and geometry, condensation rate, operating conditions etc. Moreover, film condensation and droplet condensation can coexist on the same surface.

At a constant mean overall heat transfer coefficient U_{mean}, the calculated mean heat transfer coefficient h_{mean} on the heating/evaporation side takes its maximum value, if film condensation is assumed. However, $h_{heat/evap,mean}$ reaches a minimum, if the thermal resistance of condensation is neglected. The calculated results for these two cases are displayed in Table 4. Due to the fact that the experimental condensation regime is unknown, the experimental mean heat transfer coefficients for heating or evaporation $h_{heat/evap,mean}$ can take values somewhere between the theoretical values presented in Table 4. For example, one can conclude, that the value for $h_{evap,mean}$ is between 4361 and 15,934 at operating point “evaporation 2”. A more accurate prediction is only possible, if the condensation process is known.

Solving the ODE system and the additional algebraic equations leads not only to the mean values presented in Tables 3 and 4. During simulation mass and energy balances, as well as local fluid properties and local thermal resistances (or heat transfer coefficients) are calculated. Fig. 3 exemplarily illustrates the local thermal resistance for operating point “evaporation 2”. It is a matter of course that the thermal resistance of conduction is constant along the x-coordinate. The falling film is first heated to evaporation temperature. The thermal resistance for heating R_{heat} is almost constant, because the mass flow is constant and the temperature difference from inlet to evaporation temperature is small and has no significant effect on the fluid properties (viscosity) which are affecting the local Reynolds number $Re_{F,FF}$ and therefore the local heat transfer coefficient h. The thermal resistance of evaporation R_{evap} is also almost constant. The decreasing mass flow due to evaporation leads to a decrease of the Reynolds number, but the change is quite small and has nearly no effect on the local heat transfer coefficient h. Only the transition from heating to evaporation causes a considerable change of the falling film's thermal resistance. Film condensation was assumed and the increasing thermal resistance on the condensation side R_{cond} is based on the increasing film thickness of the condensate film. It is interesting to notice, that the thermal resistance of condensation R_{cond} is exceeding the thermal resistance of evaporation R_{evap}. The total thermal resistance R_{tot} is first dominated by the thermal resistance of the falling film heating R_{heat}. But after beginning of evaporation all three thermal resistances are in the same order of magnitude and the thermal resistance of conduction and condensation contribute the main part to the total thermal resistance. The

Table 3
Comparison of experimental and calculated mean overall heat transfer coefficients.

Operating point	Reynolds number inlet	Mean overall heat transfer coefficient [W/(m²K)]		
	$Re_{F,\,FF,\,in}$ [−]	Experimental $U_{exp,mean}$	Calculated (original equations) $U_{calc,orig,mean}$	Calculated (modified equations) $U_{calc,mod,mean}$
Heating 1	683	1810 ± 47.4	2738	1755
Heating 2	1063	1558 ± 39.5	2870	1590
Evaporation 1	608	3182 ± 402	2388	3191
Evaporation 2	786	3285 ± 425	2392	3295
Evaporation 3	1037	3765 ± 512	2501	3334

Table 4
Calculated mean heat transfer coefficients h based on the experimental conditions.

Operating point	Mean heat transfer coefficient [W/(m²·K)]					
	Film condensation			Without thermal resistance for condensation		
	Condensation $h_{cond,mean}$	Heating $h_{heat,mean}$	Evaporation $h_{evap,mean}$	Condensation $h_{cond,mean}$	Heating $h_{heat,mean}$	Evaporation $h_{evap,mean}$
Heating 1	14,981	2866	–	∞[a]	2126	–
Heating 2	15,302	2433	–	∞[a]	1890	–
Evaporation 1	11,830	2288	13,714	∞[a]	1716[b]	4110
Evaporation 2	13,665	2081	15,934	∞[a]	1561[b]	4361
Evaporation 3	15,225	1921	18,800	∞[a]	1441[b]	4328

[a] Approximation.
[b] Assumption: ≈75% of the value at film condensation (analog to heating.)

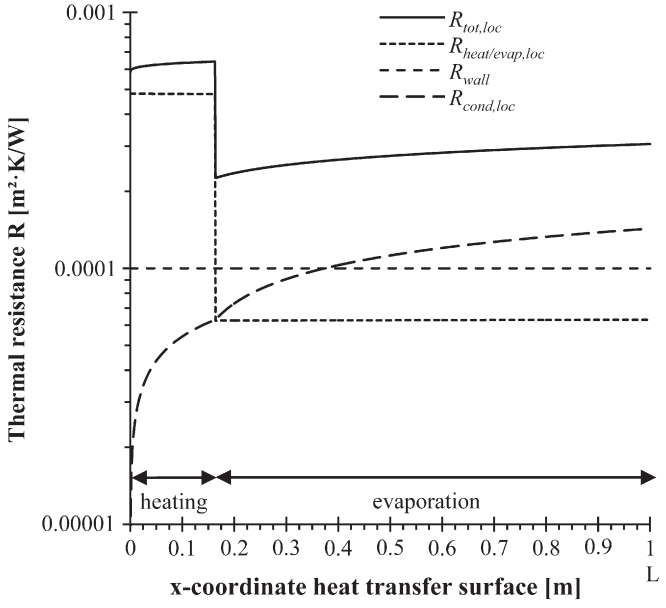

Fig. 3. Calculated local thermal resistances for the operating point "evaporation 2".

temperature difference between inlet and evaporation temperature is only about 0.65 °C. However, about 16% of the heat transfer surface is needed for falling film heating, because of the relatively high thermal resistance of heating. This leads to the conclusion that falling film pre-heating cannot be neglected for proper heat transfer modeling. The presented model was able to describe the heat transfer phenomena physically reasonable. But a better knowledge about the condensation is necessary for meaningful predictive simulations of the prototype heat exchanger. When interpreting the findings, it should be kept in mind that calculations are based on the experimental results and they contain a certain amount of uncertainty due to the measuring errors and their propagation.

5. Conclusions

The experimental results clearly demonstrate the feasibility of using heat transfer surfaces made of PEEK films. The obtained experimental mean total heat transfer coefficients are comparable to literature values of metallic falling film heat exchangers. One can conclude, that no increased heat transfer surface is necessary when using PEEK films as heat transfer surfaces in MED plants. Therefore, also peripheral installations like pumps, pipes and valves do not need to be enlarged. Besides the corrosion resistance, also the lower costs of polymer films compared to metal alloys provide an economical benefit for polymer film heat exchangers.

Heat transfer simulations of the heat exchanger revealed, that a good agreement with experimental results can only achieved, if the correlations for heat transfer coefficients on a plane wall are modified. This is necessary because the spacer alters the hydrodynamic and thermal conditions significantly. Anyway, a detailed knowledge about the condensation regime is indispensable for a more accurate model and for reliable predictive calculations. Hence, further investigations should focus on condensation on PEEK films.

Symbols

a	volume related heat transfer surface, m²/m³
A	heat transfer surface, m²
b	width of the heat transfer surface, m
c	depth of the heat transfer element, m
c_p	heat capacity at constant pressure, J/(kg·K)
g	gravitational acceleration, m/s²
h	heat transfer coefficient, W/(m²·K)
k	thermal conductivity, W/(m·K)
L	length of the heat transfer surface, m
$\dot{m}$	mass flow, kg/s
n	number of heat transfer surfaces, –
p	pressure, Pa
Pr	Prandtl number, –
Q	heat flow rate, J/s
R	area related thermal resistance, m²·K/W
Re_F	Reynolds number of the liquid falling film, –
S	wall thickness, m
u	velocity, m/s
U	overall heat transfer coefficient, W/(m²·K)
x	cartesian coordinate, m

Greek letters

Γ	liquid load, kg/(m·s)
δ	liquid film thickness, m
Δh_V	enthalpy of evaporation, J/kg
Δp	pressure difference, Pa
$\Delta\vartheta$	temperature difference, °C
ε	phase hold-up, –
η	dynamic viscosity, Pa·s
ϑ	temperature, °C
ν	kinematic viscosity, m²/s
ρ	density, kg/m³

Indices

calc	calculated
CF	condensate film (on condensation side)
cond	condensation, condensation side
evap	evaporation, evaporation side
exp	experimental
F	liquid film
FF	falling film (on evaporation side)
G	gas, gas phase
heat	heating

in	inlet
L	liquid, liquid phase
lam	laminar
loc	local
log	logarithmic
max	maximum
mean	mean
min	minimum
mod	modified
orig	original
S	heating steam (on condensation side)
tot	total
turb	turbulent
V	vapor (on evaporation side)
wall	wall, heat transfer surface

Acknowledgements

The project (240 ZN) was funded by the Federal Ministry of Economics and Technology (BMWi) through the German Federation of Industrial Research Associations (AiF).

References

[1] G. Kronenberg, F. Lokiec, Low-temperature distillation processes in single- and dual-purpose plants, Desalination 136 (2001) 189–197.
[2] C. Sommariva, H. Hogg, K. Callister, Forty-year design life: the next target material selection and operating conditions in thermal desalination plants, Desalination 136 (2001) 169–176.
[3] J.B.P. Christmann, L.J. Krätz, H.-J. Bart, Novel polymer film heat exchangers for seawater desalination, Desalin. Water Treat. 21 (2010) 162–174.
[4] H. Domininghaus, P. Elsner, P. Eyerer, T. Hirth, Kunststoffe, Springer-Verlag, Berlin Heidelberg, 2008.
[5] H. Batzer (Ed.), Polymere Werkstoffe, Band 1: Chemie und Physik, Georg Thieme Verlag, Stuttgart New York, 1985.
[6] T.B. Scheffler, A.J. Leao, Fabrication of polymer film heat transfer elements for energy efficient multi-effect distillation, Desalination 222 (2008) 707–721.
[7] L. Chen, Z. Li, Z.-Y. Guo, Experimental investigation of plastic finned-tube heat exchangers, with emphasis on material thermal conductivity, Exp. Therm. Fluid Sci. 33 (2009) 922–928.
[8] P. Luckow, A. Bar-Cohen, P. Rodgers, J. Cevallos, Energy efficient polymers for gas–liquid heat exchangers, J. Energy Resour. Technol. 132 (2010) 021001–021009.
[9] E.W. Lemmon, M.O. LcLinden, D.G. Friend, Thermophysical properties of fluid systems, NIST Chemistry WebBook, NIST Standard Reference Database Number 69, National Institute of Standards and Technology, Gaithersburg, Nov 3th 2010, http://webbook.nist.gov.
[10] VDI-Gesellschaft Verfahrenstechnik und Chemieingenieurwesen (Ed.), VDI-Wärmeatlas, Springer-Verlag, Berlin Heidelberg, 2006.
[11] W. Wagner, A. Kruse, Properties of water and steam — the industrial standard IAPWS-IF97, Springer-Verlag, Berlin, 1998.
[12] W. Nusselt, Die Oberflächenkondensation des Wasserdampfes, VDI-Zeitschrift 60 (1916) 542–575.
[13] H.D. Baehr, K. Stephan, Wärme- und Stoffübertragung, Springer-Verlag, Berlin Heidelberg, 2008.
[14] G. Schnabel, E.U. Schlünder, Wärmeübergang von senkrechten Wänden an nichtsiedende und siedende Rieselfilme, VT Verfahrenstechnik 14 (1980) 79–83.
[15] F. Kafi, V. Renaudin, D. Alonso, J.M. Hornut, A. Weber, Experimental study of a three-effect plate evaporator: seawater tests in La Spezia, Desalination 182 (2005) 175–186.
[16] F. Kafi, V. Renaudin, D. Alonso, J.M. Hornut, New MED plate desalination process: thermal performances, Desalination 166 (2004) 53–62.
[17] A.M. El-Dessouky, I. Alatiqi, S. Bingulac, H. Ettouney, Steady-state analysis of multiple-effect evaporation desalination process, Chem. Eng. Technol. 21 (1998) 437–451.
[18] A.M. El-Nashar, Predicting part load performances of small MED evaporators — a simple simulation program and its experimental verification, Desalination 130 (2000) 217–234.
[19] M. Al-Shammiri, M. Safar, Multi-effect distillation plants: state of the art, Desalination 126 (1999) 45–59.
[20] H. Raach, J. Mitrovic, Seawater falling film evaporation on vertical plates with turbulence wires, Desalination 183 (2005) 307–316.
[21] W.M. Salvagnini, M.E.S. Taqueda, A falling-film evaporator with film promotors, Ind. Eng. Chem. Res. 43 (2004) 6832–6835.
[22] W. Kast, Wärmeübertragung bei der Tropfenkondensation, Chem. Ing. Tech. 35 (1963) 163–168.
[23] S. Krischer, U. Grigull, Mikroskopische Untersuchung der Tropfenkondensation, Wärme- und Stoffübertragung 4 (1971) 48–59.